



BerryPI: A software for studying polarization of crystalline solids with WIEN2k density functional all-electron package

S.J. Ahmed^{*}, J. Kivinen, B. Zaporzan, L. Curiel, S. Pichardo, O. Rubel

Thunder Bay Regional Research Institute, 290 Munro St, Thunder Bay, Ontario, Canada
Lakehead University, 955 Oliver Road, Thunder Bay, Ontario, Canada

ARTICLE INFO

Article history:

Received 13 October 2012

Accepted 30 October 2012

Available online 6 November 2012

Keywords:

Berry phase

Density functional theory

Linearized augmented plane wave

Polarization

Effective charge

ABSTRACT

We present a module that enables computation of polarization using density functional theory based on the full potential linearized augmented plane wave package WIEN2k. The theoretical background of deriving microscopic polarization of materials using the modern theory of polarization (geometric Berry phase approach) is reviewed. The software is validated and then applied to determine spontaneous polarization and Born effective charges of several crystal structures, which are commonly studied theoretically and experimentally.

© 2012 Elsevier B.V. All rights reserved.

1. Introduction

First-principle microscopic theories, such as the density functional theory (DFT), play a major role in the development of parameter-free models that establish a relation between atomic structure and material properties using a minimum or no experimental input at all. Combined with the recent advances in high-performance computing, this development opens new opportunities in exploring novel materials and understanding their properties [1,2]. In particular, the ability of DFT to capture microscopic polarization [3–5] enables calculation of the related material properties, such as spontaneous polarization and Born effective charge [4], permittivity [6], pyroelectric coefficient [7], and piezoelectric tensor [8,9].

According to the modern theory of polarization, the polarization of a material is not a bulk property and it is ill defined [5,7]. Instead, the material properties are related to the *change* of polarization $\Delta\mathbf{P}$ in response to an external perturbation [7]

$$\Delta\mathbf{P} = \mathbf{P}^{(1)} - \mathbf{P}^{(0)} = \Omega^{-1} \int dt \int_{\text{cell}} d\mathbf{r} \mathbf{j}(\mathbf{r}, t), \quad (1)$$

where $\mathbf{j}(\mathbf{r}, t)$ is the local transient current density resulting from a charge redistribution inside the bulk unit cell. The polarization of a given state consists of two components: ionic and electronic

$$\mathbf{P} = \mathbf{P}_{\text{ion}} + \mathbf{P}_{\text{el}}. \quad (2)$$

The calculation of the ionic contribution is straightforward; it is based on the position of atomic nuclei and the corresponding ionic charges [5]. The electronic part is related to the spatial distribution of the electron density [7], which can be expressed in terms of a geometric phase (Berry phase) [3,10].

The calculation of polarization using the Berry phase is now implemented in major solid-state DFT packages, such as ABINIT [11] and VASP [12], which belong to the plane wave family. To the best of our knowledge, only one successful realization of the Berry phase approach using the all-electron full-potential linearized augmented plane wave (LAPW) method has been reported so far [8]. However, the package is not available for external users.

The purpose of this communication is to present a new software BerryPI that extends the capability of the popular all-electron full-potential DFT package WIEN2k [13] to calculation of polarization in solids using the Berry phase approach. BerryPI also relies on the WIEN2WANNIER [14] program in computing of overlap matrices as described below. As an example, we calculated the spontaneous polarization and Born effective charges of several perovskite, zinc-blende and rock-salt structures and compare the results with experimental data, pseudopotential calculations and other DFT results reported in literature.

2. Method

We consider a periodic insulating crystal, which is represented by a unit cell with N atoms and M doubly-occupied bands (non-spin-polarized calculation is considered). It is assumed that the electronic ground state can be described by a single-particle

^{*} Corresponding author at: Thunder Bay Regional Research Institute, 290 Munro St, Thunder Bay, Ontario, Canada. Tel.: +1 807 7663350.

E-mail addresses: sjaonline@gmail.com (S.J. Ahmed), rubelo@tbh.net (O. Rubel).

mean-field Hamiltonian as in the density-functional theory. The eigenstates of this Hamiltonian are the Bloch functions

$$\psi_{n\mathbf{k}}(\mathbf{r}) = u_{n\mathbf{k}}(\mathbf{r})e^{i\mathbf{k}\cdot\mathbf{r}}, \quad (3)$$

which are characterized by the band-index n and the wave vector \mathbf{k} . The cell-periodic complex amplitude $u_{n\mathbf{k}}(\mathbf{r}) = u_{n\mathbf{k}}(\mathbf{r} + \mathbf{R})$ remains invariant for any lattice vector \mathbf{R} .

The total microscopic polarization of such a system is given by [3]

$$\mathbf{P} = \frac{e}{\Omega} \sum_s^{\text{atoms}} Z_s^{\text{ion}} \mathbf{r}_s - \frac{2ei}{(2\pi)^3} \sum_n^{\text{occ. bands}} \int_{\text{BZ}} d\mathbf{k} \langle u_{n\mathbf{k}} | \nabla_{\mathbf{k}} | u_{n\mathbf{k}} \rangle, \quad (4)$$

where Ω is the simulation cell volume, e is the elementary charge, Z_s^{ion} is the ionic charge represented by the number of valence electrons in the atom s and \mathbf{r}_s is its position vector. The factor of 2 in the numerator corresponds to the band occupancy. The integration in Eq. (4) is performed over the Brillouin zone (BZ), and the integrand is closely related to the geometrical phase change [10]

$$d\varphi_n = -i \langle u_{n\mathbf{k}} | \nabla_{\mathbf{k}} | u_{n\mathbf{k}} \rangle \cdot d\mathbf{k} = -i \ln \langle u_{n\mathbf{k}} | u_{n(\mathbf{k}+d\mathbf{k})} \rangle. \quad (5)$$

After summation over all occupied bands, the integral in Eq. (4) will represent an average phase acquired by system wavefunctions, i.e. the electronic phase. This phase value has the uncertainty of an integer multiple of 2π .

The Cartesian α component of total polarization of a state can be expressed in terms of the corresponding total phase Φ_α [9]

$$P_\alpha = \frac{e}{\Omega} \frac{\Phi_\alpha}{2\pi} R_\alpha \quad (6)$$

where R_α is the length of the real-space lattice vector in the direction α . By analogy with Eq. (4) for polarization, the total phase is split into two components

$$\Phi_\alpha = \varphi_{\text{el},\alpha} + \varphi_{\text{ion},\alpha}, \quad (7)$$

where $\varphi_{\text{el},\alpha}$ and $\varphi_{\text{ion},\alpha}$ are electronic and ionic phases, respectively.

The ionic phase for a given structure is determined by the spatial position and charge of individual ions via [9]

$$\varphi_{\text{ion},\alpha} = 2\pi \sum_{s=1}^N Z_s^{\text{ion}} \rho_{s,\alpha}, \quad \text{wrapped in the range } [0, 2\pi] \quad (8)$$

where $\rho_{s,\alpha}$ is the fractional coordinate of ion s in the crystallographic direction α .

In practice, the Berry phase $\varphi(\mathbf{k}_\parallel)$ is computed for individual k -paths parallel to the α -axis in the Brillouin zone (Fig. 1), and each result is wrapped in the range of $[0, 2\pi]$. Then, the total electronic phase corresponds to an average [3]

$$\varphi_{\text{el},\alpha} = S_\perp^{-1} \int_{S_\perp} dS_\perp \varphi(\mathbf{k}_\parallel), \quad (9)$$

where S_\perp is the surface area of the Brillouin zone perpendicular to the α -axis. The Berry phase for an individual path \mathbf{k}_\parallel can be expressed as [3]

$$\varphi(\mathbf{k}_\parallel) = 2 \text{Im} \left[\ln \prod_{j=0}^{J-1} \det \mathbb{S}_{M \times M}(\mathbf{k}_j, \mathbf{k}_{j+1}) \right]. \quad (10)$$

Here \mathbb{S} is the overlap matrix of size M^2 , where M is the number of occupied bands, and the factor of two takes into account the spin degeneracy. The path is designed such that the end k -point represents the starting point displaced by the reciprocal lattice vector, i.e., $\mathbf{k}_J - \mathbf{k}_0 = \mathbf{G}_\alpha$.

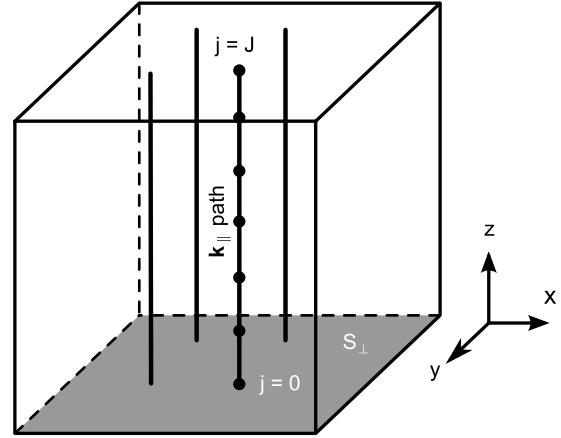


Fig. 1. Berry phase integration in the Brillouin zone for calculation of the electronic polarization along the z -axis.

Computation of the overlap integral between two cell periodic parts of the Bloch function

$$\mathbb{S}_{mn}(\mathbf{k}_j, \mathbf{k}_{j+1}) = \langle u_{m\mathbf{k}_j} | u_{n\mathbf{k}_{j+1}} \rangle \quad (11)$$

is the most challenging part in determining the Berry phase. Here m and n refer to the occupied band indices, which span in the range 1 to M . Calculation of such an integral is a part of the standard procedure of constructing Wannier functions, which is done by the WIEN2WANNIER package [14].

3. Program implementation

BerryPI is a Python script that controls the execution process according to the flow in Table 1. The script is invoked in the case directory after completing the standard WIEN2k self-consistency field cycle. The only input parameter required is the \mathbf{k} -mesh for Berry phase integration. The script determines the number of occupied bands M , cell geometry, the ionic charges and their relative positions based on WIEN2k files. The electronic, ionic and total phases as well as the corresponding components of polarization are calculated along the Cartesian axes.

Since the ionic and electronic phases used in the calculation of polarization carry the uncertainty of an integer multiple of 2π , the proper calculation of the polarization difference between two structures requires $\Delta P \lesssim |eR/\Omega|$. In the case of typical perovskite structures, $|eR/\Omega|$ is of the order of 1 C/m², which is still greater than typical values of the spontaneous polarization (see Table 3).

When comparing the polarization between two structures, it is useful to inspect the total phases as shown in Fig. 2. In this specific case, the phases are $\Phi^{(0)} = -0.9\pi$ and $\Phi^{(1)} = +0.9\pi$, which yields $\Delta\Phi^{(1-0)} = 1.8\pi$ instead of -0.2π . This ambiguity can be resolved by performing a calculation for the third structure, which represents an intermediate state between (0) and (1).

The source code of BerryPI can be downloaded from the GitHub repository. The execution of BerryPI requires WIEN2k [13] and WIEN2WANNIER [14] installed along with Python and the NumPy library.

4. Validation

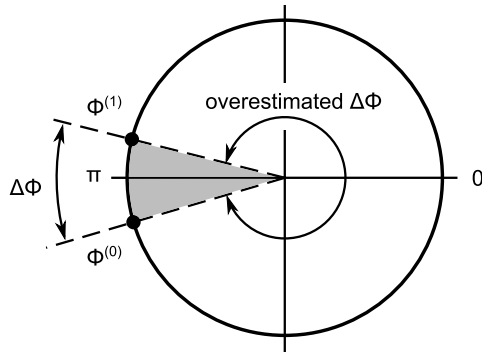
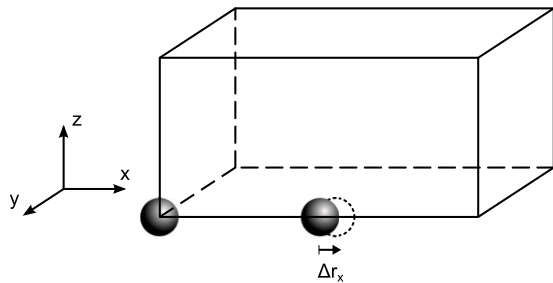
First, we begin with calculation of polarization in the case where the outcome can be predicted exactly. For non-interacting (noble) atoms the net polarization is zero. Therefore the electronic and ionic polarization should cancel each other, $P_{\text{ion}} + P_{\text{el}} = 0$. This property is used in order to test the accuracy of our calculations of polarization.

Table 1
Calculation flow.

Command	Description	Input files	Output files	Package
x kgen -fbz	Generates a k -mesh in the full Brillouin zone	kgen.def case.struct	case.outputkgen case.klist case.kgen	WIEN2k
write_w2win case	Prepare the input for w2w with the occupied band range ^a	case.struct case.outputkgen	case.w2win	WIEN2WANNIER
write_win case	Create the input file for w2w	case.struct case.outputkgen case.klist case.w2win	case.win	WIEN2WANNIER
win2nnkp.py case	Generate the nearest neighbor list of k -points	case.win	case.nnkp	BerryPI
write_w2wdef case	Create definition file for w2w	–	w2w.def	WIEN2WANNIER
x lapw1 (-c)	Calculate wavefunctions for the new k -list	case.struct case.klist	case.vector case.energy	WIEN2k
w2w case	Calculate the overlap matrix $S_{mn}(\mathbf{k}_j, \mathbf{k}_{j+1})$	case.struct case.nnkp case.vector case.ensp case.vsp case.w2win case.dayfile	case.mmn	WIEN2WANNIER
mmn2pathphase.py case x	Calculate the Berry phase along x-axis ^b	case.mmn case.win	case-x.pathphase	BerryPI

^a The range of bands from 1 to the last occupied band is taken from case.scf file.

^b x, y or z are used to specify the Cartesian axes along which the Berry phase is calculated.

**Fig. 2.** Phase map that illustrates two ways of computing the phase difference $\Delta\Phi$.**Fig. 3.** The unit cell containing two noble atoms used for the test. One of the atoms is displaced from its centrosymmetric position.

Two helium atoms were placed in a tetragonal cell as illustrated in Fig. 3. The cell dimensions $a = 10$ and $b = c = 5$ Bohr were chosen in order to prevent a possible interaction between neighboring atoms. The reference structure had one atom positioned in the origin, while the second atom was placed at $\rho_x = 0.5$, $\rho_y = \rho_z = 0$. In the perturbed structure, the second atom was slightly displaced in the x direction.

Table 2
Test for noble atoms.

Element	Displacement	Change in the polarization ($\text{C}/\text{m}^2 \times 10^{-3}$)	
		ΔP_{ion}	ΔP_{el}
He	0.001a	4.5802	-4.5814
	0.002a	9.1604	-9.1604
	0.005a	22.8966	-22.9058
Ne	0.001a	-18.3210	18.3234
	0.05a	-916.0496	916.0496

The standard self-consistency LAPW cycle was executed with WIEN2k for both structures using one k -point. It is strongly advised *not* to use an iterative diagonalization option in the self-consistency cycle prior to the Berry calculation, as it will likely lead to spurious results. We forced WIEN2k to preserve the symmetry of a perturbed structure when performing the calculation for the reference (centrosymmetric) case. Then we calculate the electronic and ionic polarization for both structures following the steps described in Table 1 using a $10 \times 1 \times 1$ k -mesh. The fine mesh in the x direction is required for accurate computation of the Berry phase in Eq. (10).

Results of the calculated difference in polarization between the reference and perturbed structures are presented in Table 2. It is apparent that the ionic and electronic polarization cancel each other with high accuracy even for very small perturbations. The same calculations were repeated for neon in order to verify the performance in the case of multiple bands and core electrons. The results for the ionic and electronic polarization (Table 2) are also consistent with the expectation of zero net polarization, which validates our approach. The sign alternation between the ionic and electronic components of polarization is due to 2π wrapping applied to the phase.

5. Applications

In the following, we provide two examples on calculation of the material properties related to polarization using BerryPI.

Table 3
Spontaneous polarization (C/m²) for perovskite compounds.

Compound	BerryPI	ABINIT	Experimental	Other calculations
BaTiO ₃	0.31	0.28	0.26 ^a	0.22 ^b , 0.29 ^c
KNbO ₃	0.36	0.34	0.37 ^d	0.33 ^e
PbTiO ₃	0.86	0.84	0.75 ^f	0.88 ^g

^a Wieder [19].

^b Fechner et al. [20]: Projector augmented waves, with the local density approximation (LDA) for the exchange–correlation functional.

^c Wang et al. [21]: projector augmented waves, LDA.

^d Kleemann et al. [22].

^e Wang et al. [23]: LAPW (linear response), LDA.

^f Gavrilachenko [24].

^g Sághi-Szabó et al. [8]: LAPW-GGA.

The examples include modeling the spontaneous polarization of perovskite crystals and calculation of the Born effective charge of polar materials.

5.1. Spontaneous polarization

Spontaneous polarization P_s is one of the major characteristics for ferroelectric materials. It is defined as the change in polarization that occurs when the crystal undergoes a phase change from the centrosymmetric structure to a structure without an inversion symmetry

$$P_s = P_{nc} - P_c. \quad (12)$$

Here P_{nc} and P_c refer to the polarization values for non-centrosymmetric and centrosymmetric structures, respectively. Fig. 4 illustrates a particular example of the ABO_3 perovskite crystal in two different phases: cubic (centrosymmetric) and tetragonal (non-centrosymmetric).

For our study we selected some of the most well characterized perovskite compounds: BaTiO₃, KNbO₃ and PbTiO₃. The calculations were performed with the WIEN2k package using the generalized gradient approximation [15] (GGA) for the exchange correlation functional and $6 \times 6 \times 6$ sampling of the Brillouin zone. The radii R_{MT} of muffin tin spheres centered around individual atoms are chosen to be equal: 2.5, 2.5, 2.26, 1.77, 1.7 and 1.5 Bohr for Ba, K, Pb, Nb, Ti and O, respectively. The product of the minimum R_{MT} radius and the maximum cut-off wave vector in the reciprocal space was kept at a constant value of $R_{MT}K_{max} = 7$ throughout all calculations. The energy to separate core and valence electrons was set such that electrons in the following orbitals were treated as valence electrons: Ba—5s 5p 6s, K—3s 3p 4s, Pb—4f 5d 6s 6p, Nb—4s 4p 4d 5s, Ti—3s 3p 3d 4s and O—2s 2p. In order to minimize the discrepancy between experimental and theoretical structures, we adopted the experimental values [16–18] of the lattice constant for all three compounds in our calculations. The internal degrees of freedom for tetragonal structures were fully relaxed by minimizing the Hellmann–Feynman forces acting on atoms below 0.2 mRy/Bohr. The convergence tests performed with a denser k -mesh $10 \times 10 \times 10$ and $R_{MT}K_{max} = 8$ indicate that the polarization calculations itself are not sensitive to those parameters (only 0.3% difference). However, a special care should be taken to obtain accurate atomic positions. This is why the force convergence criteria is reduced down to 0.2 mRy/Bohr, which is less than the default value by a factor of 10.

Results of our calculations of the spontaneous polarization in BaTiO₃, KNbO₃ and PbTiO₃ compounds are summarized in Table 3. Our results are consistent with the experimental data and results of other first-principle calculations.

Next we explore the sensitivity of calculation results to the choice of the basis set (LAPW vs. plane waves). The same calculations were repeated with the ABINIT package [11] using Hartwigsen–Goedecker–Hutter pseudopotentials with semicore

Table 4
Born effective charge Z_{zz}^* for tetragonal perovskite crystals.

Compound	Atom	BerryPI	Other calculations ^a
BaTiO ₃	Ba	+2.77	+2.83
	Ti	+5.90	+5.81
	O1	−4.79	−4.73
	O2	−1.97	−1.95
PbTiO ₃	O3	−1.97	−1.95
	Pb	+3.50	+3.52
	Ti	+5.34	+5.18
PbTiO ₃	O1	−4.51	−4.38
	O2	−2.14	−2.16
	O3	−2.14	−2.16
GaAs	As	−2.21	−2.00
NaCl	Na	+1.11	+0.99

^a Results for BaTiO₃ are based on pseudopotential DFT-LDA calculations [26]. The data for PbTiO₃ refer to LAPW DFT-GGA calculations [8]. GaAs values were obtained from pseudopotential DFT-LDA calculations [28]. The effective charges for NaCl refer to Hartree–Fock calculations [29].

electrons for K, Ti, Nb and Ba [25]. Due to the presence of semicore electrons, the cutoff energy was chosen to be relatively high (30 Ha). In this calculation the k -mesh, lattice parameters and atomic positions were kept identical to those used in WIEN2k. Our ABINIT results (Table 3) are in agreement with LAPW (BerryPI) data within 10% accuracy range.

5.2. Born effective charge

The Born effective charge reveals the mixed ionic and covalent character of bonds and provides further insight into understanding the origin of polarization effects in solids [26]. By definition, the Born effective charge of an atom in a solid is related to the change in polarization due to the displacement of this atom from its equilibrium position [27]

$$Z_{s,\alpha\beta}^* = \frac{\Omega}{e} \frac{\partial P_\alpha}{\partial r_{s,\beta}}. \quad (13)$$

It is convenient to express the effective charge in terms of the total phase using Eq. (6), which yields

$$Z_{s,\alpha\beta}^* = (2\pi)^{-1} \frac{\partial \Phi_\alpha}{\partial \rho_{s,\beta}}. \quad (14)$$

The zz component of the Born effective charge tensor was calculated for tetragonal BaTiO₃ and PbTiO₃ structures using the same parameters as described in Section 5.1. Individual atoms were displaced by $\rho_{s,z} = \pm 0.01$, while keeping the position of other atoms unchanged. The self-consistent electron density was obtained for each perturbation. The corresponding change of the total phase along the z axis was used in order to compute the derivative in Eq. (14). The calculated Born effective charges are presented in Table 4. The results obey the acoustic sum rule $\sum_s Z_{s,\alpha\beta}^* = 0$ with a negligible error. We also report calculation of the effective charge for binary zinc-blende (GaAs) and rock-salt (NaCl) structures. Our data are also consistent with results of other first-principle calculations listed in Table 4.

6. Conclusions

We presented a module that extends the capability of WIEN2k (all-electron density functional package) to calculation of polarization using the Berry phase approach. The accuracy of calculations was verified using a model of non-interacting noble atoms. We applied the approach to calculation of spontaneous polarization and Born effective charge of some well characterized perovskite crystals, sodium chloride and zinc-blende structures. Obtained

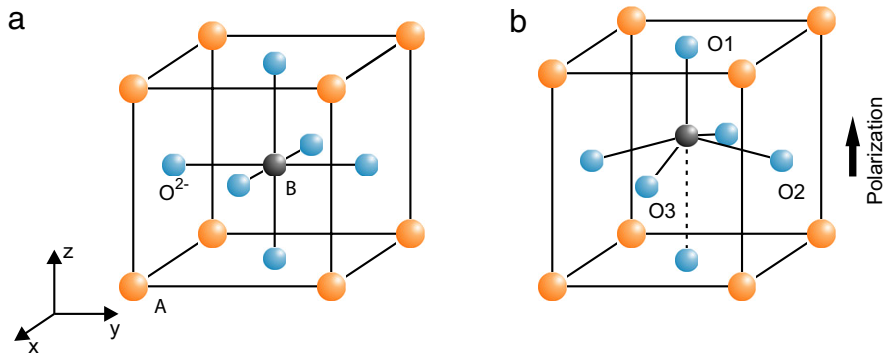


Fig. 4. (Color online) Perovskite ABO_3 cubic (a) and tetragonal (b) crystal structures.

results agree with alternative calculations and experimental data.

Acknowledgments

The authors would like to thank Dr. Peter Blaha for stimulating discussions, critical reading of the manuscript and editorial suggestions. The authors also want to acknowledge funding provided by the Natural Sciences and Engineering Research Council of Canada under the Discovery Grant Program “Microscopic theory of high-field transport in disordered semiconductors”, the Ontario Ministry of Economic Development and Innovation under the Ontario Research Fund program and the Thunder Bay Community Economic and Development Commission.

References

- [1] K. Rabe, *Nature Mater.* 1 (2002) 147.
- [2] R.F. Service, *Science* 335 (2012) 1434.
- [3] R.D. King-Smith, D. Vanderbilt, *Phys. Rev. B* 47 (1993) 1651.
- [4] R. Resta, M. Posternak, A. Baldereschi, *Phys. Rev. Lett.* 70 (1993) 1010.
- [5] R. Resta, *Rev. Modern Phys.* 66 (1994) 899.
- [6] F. Bernardini, V. Fiorentini, D. Vanderbilt, *Phys. Rev. Lett.* 79 (1997) 3958.
- [7] R. Resta, D. Vanderbilt, *Theory of polarization: a modern approach*, in: *Physics of Ferroelectrics*, in: *Topics Appl. Physics*, vol. 105, Springer Verlag, Berlin, Heidelberg, 2007, pp. 31–68 (Chapter).
- [8] G. Sághi-Szabó, R.E. Cohen, H. Krakauer, *Phys. Rev. Lett.* 80 (1998) 4321.
- [9] D. Vanderbilt, *J. Phys. Chem. Solids* 61 (2000) 147.
- [10] M.V. Berry, *Proc. R. Soc. Ser. A* 392 (1984) 45.
- [11] X. Gonze, J.-M. Beuken, R. Caracas, F. Detraux, M. Fuchs, G.-M. Rignanese, L. Sindic, M. Verstraete, G. Zerah, F. Jollet, et al., *Comput. Mater. Sci.* 25 (2002) 478.
- [12] G. Kresse, J. Furthmüller, *Comput. Mater. Sci.* 6 (1996) 15.
- [13] P. Blaha, K. Schwarz, G.K.H. Madsen, D. Kvasnicka, J. Luitz, *Wien2k: an augmented plane wave + local orbitals program for calculating crystal properties*, Karlheinz Schwarz, Techn. Universität Wien, Austria, 2001.
- [14] J. Kunes, R. Arita, P. Wissgott, A. Toschi, H. Ikeda, K. Held, *Comput. Phys. Comm.* 181 (2010) 1888.
- [15] J.P. Perdew, K. Burke, M. Ernzerhof, *Phys. Rev. Lett.* 77 (1996) 3865.
- [16] F. Jona, G. Shirane, *Ferroelectric Crystals*, Dover, New York, 1993.
- [17] G.H. Kwei, A.C. Lawson, S.J.L. Billinge, S.W. Cheong, *J. Phys. Chem.* 97 (1993) 2368.
- [18] A.W. Hewat, *J. Phys. C* 6 (1973) 2559.
- [19] H.H. Wieder, *Phys. Rev.* 99 (1955) 1161.
- [20] M. Fechner, S. Ostanin, I. Mertig, *Phys. Rev. B* 77 (2008) 094112.
- [21] J.J. Wang, F.Y. Meng, X.Q. Ma, M.X. Xu, L.Q. Chen, *J. Appl. Phys.* 108 (2010) 034107.
- [22] W. Kleemann, F.J. Schäfer, M.D. Fontana, *Phys. Rev. B* 30 (1984) 1148.
- [23] C.-Z. Wang, R. Yu, H. Krakauer, *Ferroelectrics* 194 (1997) 97.
- [24] V. Gavrilachenko, *Sov. Phys. Solid State* 12 (1970) 1203.
- [25] C. Hartwigsen, S. Goedecker, J. Hutter, *Phys. Rev. B* 58 (1998) 3641.
- [26] P. Ghosez, J.-P. Michenaud, X. Gonze, *Phys. Rev. B* 58 (1998) 6224.
- [27] M. Born, K. Huang, *Dynamical Theory of Crystal Lattices*, University Press, Oxford, 1968.
- [28] T. Sengstap, N. Binggeli, A. Baldereschi, *Phys. Rev. B* 52 (1995) R8613.
- [29] A. Shukla, *Phys. Rev. B* 61 (2000) 13277.